

Extra-narrowband metallic filters with an ultrathin single-layer metallic grating

Ran Wang(王然), Qi-Huang Gong(龚旗煌), Jian-Jun Chen(陈建军)

Citation: Chin. Phys. B . 2020, 29(6): 064215 . **doi:** 10.1088/1674-1056/ab8899
Journal homepage: http://cpb.iphy.ac.cn; http://iopscience.iop.org/cpb

What follows is a list of articles you may be interested in

Design of diamond-shape photonic crystal fiber polarization filter based on surface plasma resonance effect

Yongxia Zhang(张永霞), Jinhui Yuan(苑金辉), Yuwei Qu(屈玉玮), Xian Zhou(周娴), Binbin Yan(颜玢玢), Qiang Wu(吴强), Kuiru Wang(王葵如), Xinzhu Sang(桑新柱), Keping Long(隆克平), Chongxiu Yu(余重秀)

Chin. Phys. B . 2020, 29(3): 034208 . **doi:** 10.1088/1674-1056/ab683c

Dynamically adjustable asymmetric transmission and polarization conversion for linearly polarized terahertz wave

Tong Li(李彤), Fang-Rong Hu(胡放荣), Yi-Xian Qian(钱义先), Jing Xiao(肖靖), Long-Hui Zhang(张隆辉), Wen-Tao Zhang(张文涛), Jia-Guang Han(韩家广)

Chin. Phys. B . 2020, 29(2): 024203 . **doi:** 10.1088/1674-1056/ab5ef8

Selective synthesis of three-dimensional ZnO@Ag/SiO_2@Ag nanorod arrays as surface-enhanced Raman scattering substrates with tunable interior dielectric layer

Jia-Jia Mu(牟佳佳), Chang-Yi He(何畅意), Wei-Jie Sun(孙伟杰), Yue Guan(管越)

Chin. Phys. B . 2019, 28(12): 124204 . **doi:** 10.1088/1674-1056/ab4d45

Electrically triggered dual-band tunable terahertz metamaterial band-pass filter based on Si_3N_4-VO_2-Si_3N_4 sandwich

Shuai Zhao(赵帅), Fangrong Hu(胡放荣), Xinlong Xu(徐新龙), Mingzhu Jiang(江明珠), Wentao Zhang(张文涛), Shan Yin(银珊), Wenying Jiang(姜文英)

Chin. Phys. B . 2019, 28(5): 054203 . **doi:** 10.1088/1674-1056/28/5/054203

Tunable graphene-based mid-infrared band-pass planar filter and its application

Somayyeh Asgari, Hossein Rajabloo, Nosrat Granpayeh, Homayoon Oraizi

Chin. Phys. B . 2018, 27(8): 084212 . **doi:** 10.1088/1674-1056/27/8/084212

Extra-narrowband metallic filters with an ultrathin single-layer metallic grating*

Ran Wang(王然)[1,2], Qi-Huang Gong(龚旗煌)[1,3,4], and Jian-Jun Chen(陈建军)[1,3,4,†]

[1] State Key Laboratory for Mesoscopic Physics, School of Physics, Peking University, Beijing 100871, China
[2] Microelectronics Instruments and Equipments R&D Center, Institude of Microelectronics of Chinese Academy of Sciences, Beijing 100029, China
[3] Nano-optoelectronics Frontier Center of Ministry of Education (NFC-MOE) & Collaborative Innovation Center of Quantum Matter, Peking University, Beijing 100871, China
[4] Collaborative Innovation Center of Extreme Optics, Shanxi University, Taiyuan 030006, China

(Received 8 March 2020; revised manuscript received 7 April 2020; accepted manuscript online 12 April 2020)

Narrowband and high-transmission optical filters are extensively used in color display technology, optical information processing, and high-sensitive sensing. Because of large ohmic losses in metallic nanostructures, metallic filters usually exhibit low transmittances and broad bandwidths. By employing both strong field enhancements in metallic nano-slits and the Wood's anomaly in a periodic metallic grating, an extra-narrowband and high-transmission metallic filter is numerically predicted in an ultrathin single-layer metallic grating. Simulation results show that the Wood's anomaly in the ultrathin (thickness $H = 60$ nm) single-layer metallic grating results in large field enhancements in the substrate and low losses in the metallic grating. As a result, the transmission bandwidth (transmittance $T > 60\%$) at $\lambda = 1200$ nm is as small as $\Delta\lambda_{\rm FWHM} = 1.6$ nm, which is smaller than 4% of that in the previous thin dielectric and metallic filters. The corresponding quality factor is as high as $Q = \lambda/\Delta\lambda_{\rm FWHM} = 750$, which is 40 times greater than that in the previous reports. Moreover, the thickness of our metallic filter ($H = 60$ nm) is smaller than 40% of that in the previous reports, and its maximum transmittance can reach up to 80%. In experiments, a narrowband metallic filter with a bandwidth of about $\Delta\lambda_{\rm FWHM} = 10$ nm, which is smaller than 25% of that in the previous metallic filters, is demonstrated.

Keywords: metallic filter, extra-narrowband, field enhancement, Wood's anomaly

PACS: 42.79.Ci, 42.79.Dj, 78.67.Pt, 81.05.Xj **DOI:** 10.1088/1674-1056/ab8899

1. Introduction

Optical filters are an important element in optical displays,[1] sensors,[2] digital photography,[3] and so on. Various filters have been proposed in recent decades, including dye or pigment filters,[4] dielectric filters,[5,6] and metallic filters.[7] Compared with conventional dye or pigment filters,[4] dielectric and metallic filters based on micro/nanostructures exhibit better ultraviolet, power, and temperature reliability. Additionally, the filtering properties of dielectric and metallic filters can be easily manipulated by geometrical dimensions, such as the shape and size of the nanostructures. However, miniaturization of dielectric filters is hampered by the diffraction limit of light. What is worse, because of small contrasts of refractive indices, reflection on an interface of different dielectric materials is very low (e.g., reflectivity $\sim 16\%$ on a Si–SiO_2 interface), making the bandwidths (full width at half-maximum, FWHM) of dielectric filters with several layers greater than 100 nm.[5,6]

Surface plasmon polaritons (SPPs) supported by metallic nanostructures are electromagnetic waves confined on metal surfaces at the visiable and infrared frequencies.[8] Due to subwavelength field confinements and large field enhancements, SPPs are promising to significantly miniaturize photonic devices.[8] Recently, various metallic nanostructures based on SPPs have been proposed to realize metallic filters, including periodic subwavelength metallic hole arrays,[9–11] metallic metasurfaces,[12–14] and metal–insulator–metal (MIM) nanoresonators.[15–17] For example, by periodically designing subwavelength hole arrays on a metal film with optical thickness, a metallic filter could be achieved based on the extraordinary optical transmission (EOT).[18] However, due to the subwavelength diameters of the hole arrays on the optical thick metal film (thickness > 150 nm), the absolute transmittance was rather low ($T < 50\%$).[9–11] Moreover, the transmission spectra were broad ($\Delta\lambda_{\rm FWHM} > 100$ nm) because of the inherent ohmic losses in metals. Metallic metasurfaces could be used to achieve reflective plasmonic filters based on resonant absorptions of gap SPP modes in MIM nanoresonators (gap thickness < 50 nm).[12,13] Although the maximum reflection peak was as high as $T = 90\%$,[14] their reflection spectra were still rather broad ($\Delta\lambda_{\rm FWHM} > 100$ nm) because of the large resonant absorptions of the MIM nanogaps.[12,13] Recently, by designing a metasurface with arrays of elliptical and circular nanoholes on an 80-nm-thick gold film, which was covered by a 300-nm-thick SiO_2 layer, the transmittance and band-

*Project supported by the National Key Research and Development Program of China (Grant Nos. 2018YFA0704401, 2017YFF0206103, and 2016YFA0203500), the National Natural Science Foundation of China (Grant Nos. 61922002, 91850103, 11674014, 61475005, 11527901, 11525414, and 91850111), and the Beijing Natural Science Foundation, China (Grant No. Z180015).

†Corresponding author. E-mail: jjchern@pku.edu.cn

© 2020 Chinese Physical Society and IOP Publishing Ltd

width were reported to be $T = 44\%$ and $\Delta\lambda_{\rm FWHM} \approx 79$ nm, respectively.[14] By using planar MIM structures (the thickness of the insulator > 100 nm), a narrowband ($\Delta\lambda_{\rm FWHM} \approx 40$ nm) metallic filter was realized based on the Fabry–Perot effect because of the high reflectance ($> 60\%$) of the metals, and the maximum transmittance was $T \approx 60\%$.[17] The thicknesses of these filters based on multilayer MIM structures were larger than 150 nm.[15–17] In the above metallic filters,[9–17] the bandwidths could not be further decreased due to the inherent ohmic losses of the metals. Therefore, it is a great challenge to realize thin metallic filters with both narrow bandwidths and high transmittances, which are important for high resolution optical imaging, dense wavelength-division-multiplexed optical information processing, and high-sensitive sensing in the micro/nano optics.

In this paper, an extra-narrowband metallic filter is numerically and experimentally demonstrated with an ultrathin (thickness $H = 60$ nm) single-layer metallic grating. When a p-polarized incident beam illuminates the one-dimensional (1D) metallic grating, huge field enhancements occur in the nano-slits, and interference of radiative fields from the periodic nano-slits gives rise to the Wood's anomaly in the thin periodic metallic grating. Unlike localized field enhancements of SPPs on metal–dielectric interfaces, the Wood's anomaly results in large field enhancements in the substrate, which efficiently reduces the ohmic losses in metals. The strong field in the substrate can pass through the nano-slits, resulting in an extra-narrowband and high-transmission filter because of the reduced ohmic losses in metals. Numerical simulation results show that a transmission peak is up to $T = 80\%$, and a transmission bandwidth at $\lambda = 1200$ nm is as small as $\Delta\lambda_{\rm FWHM} \approx 1.6$ nm, which is much smaller than that in the previous reports ($\Delta\lambda_{\rm FWHM} \geq 40$ nm).[9–17] The corresponding quality factor is as high as $Q = \lambda/\Delta\lambda_{\rm FWHM} = 750$, which is 40 times greater than that in the previous reports.[9–17] Experimentally, metallic gratings are fabricated on an ultrathin single-layer gold film, and the experimental results consist with the simulation data. Due to polycrystalline gold films and fabrication defects, the narrowest bandwidth in the experiment becomes $\Delta\lambda_{\rm FWHM} \approx 10$ nm, which is still smaller than 25% of that in the previous reports ($\Delta\lambda_{\rm FWHM} \geq 40$ nm).[9–17]

2. Simulation

The ultrathin metallic grating structure is schematically shown in Fig. 1(a). This structure comprises periodic nano-slits with a width of w and a period of P in a metallic film (thickness of H), which is placed on a K9 glass substrate. An incident beam with a p-polarization state (vacuum wavelength of λ) can excite strong SPPs in the metallic slits under back illumination from the substrate. The interference of the backward radiations from the periodic metallic nano-slits results in the Wood's anomaly in the glass substrate.[19] The resonant wavelength of the Wood's anomaly depends on resonant order m, refractive index of the substrate $n_{\rm d}$, and the grating period P,[20]

$$m\lambda = n_{\rm d}P. \tag{1}$$

The enhanced field in the substrate resulting from the Wood's anomaly can pass through the metallic nano-slit, resulting in a high transmittance.

For the verification of the analysis, a commercial software COMSOL Multiphysics is firstly adopted for simulating the transmission spectra of the nano-struectures.[21] The metal film is selected as a gold film with a thickness of $H = 60$ nm. The thickness is smaller than 40% of that in the previous dielectric and metallic filters (thickness ≥ 150 nm).[9–17] The geometric parameters of the grating are $P = 600$ nm and $w = 60$ nm. The permittivity of gold is derived from the experiment results in Ref. [22]. The substrate is K9 glass with a refractive index of $n = 1.5$. For the gold film with $H = 60$ nm, the reflection is as high as 96.3%, and the transmittance is only 0.5% at $\lambda = 900$ nm. Figure 1(b) plots the transmission spectra of the metallic grating under the normal illumination with p-polarization (electric vector parallel to x axis) and s-polarization (electric vector vertical to x axis) from the substrate. Under an incident light with p-polarization, it can be observed that the transmittance reaches to a peak of $T \approx 80\%$ at $\lambda = 900$ nm, and the bandwidth is $\Delta\lambda_{\rm FWHM} \approx 3.0$ nm. The resonant wavelength ($\lambda = 900$ nm) matches well with the first-order resonant condition ($m = 1$) of the Wood's anomaly based on Eq. (1). The normalized electric field amplitude distribution ($|E|/E_0|$) at the Wood's anomaly resonance ($\lambda = 900$ nm) is shown in Fig. 1(c). Here, $|E_0|$ is the amplitude of the electric field of the incident light. The simulation shows that a large field enhancement ($|E|/E_0| \approx 12$) occurs in the metallic nano-slits. The strong field in the metallic nano-slit leads to the forward and backward radiations. Since the refractive index ($n = 1.5$) of the glass substrate is greater than that of the air ($n = 1.0$), the simulation reveals that the backward radiation (energy flow) into the glass substrate is 2.4 times the forward radiation into the air. The interference of the backward radiations from the periodic nano-slits results in the Wood's anomaly resonance, which leads to the interference pattern with large field enhancements ($|E|/E_0| \sim 8$) in the glass substrate, as shown in Fig. 1(c). It can be seen that the interference pattern with a period of 300 nm is perpendicular to the gold film, further confirming the Wood's anomaly resonance. Since the field is mainly distributed in the glass substrate, the ohmic losses in the thin metallic grating are greatly reduced. The enhanced field in the substrate can pass through the nano-slit in the ultrathin gold film, resulting in a high transmittance ($T \approx 80\%$) and a narrow bandwidth ($\Delta\lambda_{\rm FWHM} \approx 3.0$ nm), as depicted by the black line in Fig. 1(b). The maximum transmittance ($T \approx 80\%$) is about 160 times of that ($T = 0.5\%$) of the 60 nm-think gold film.

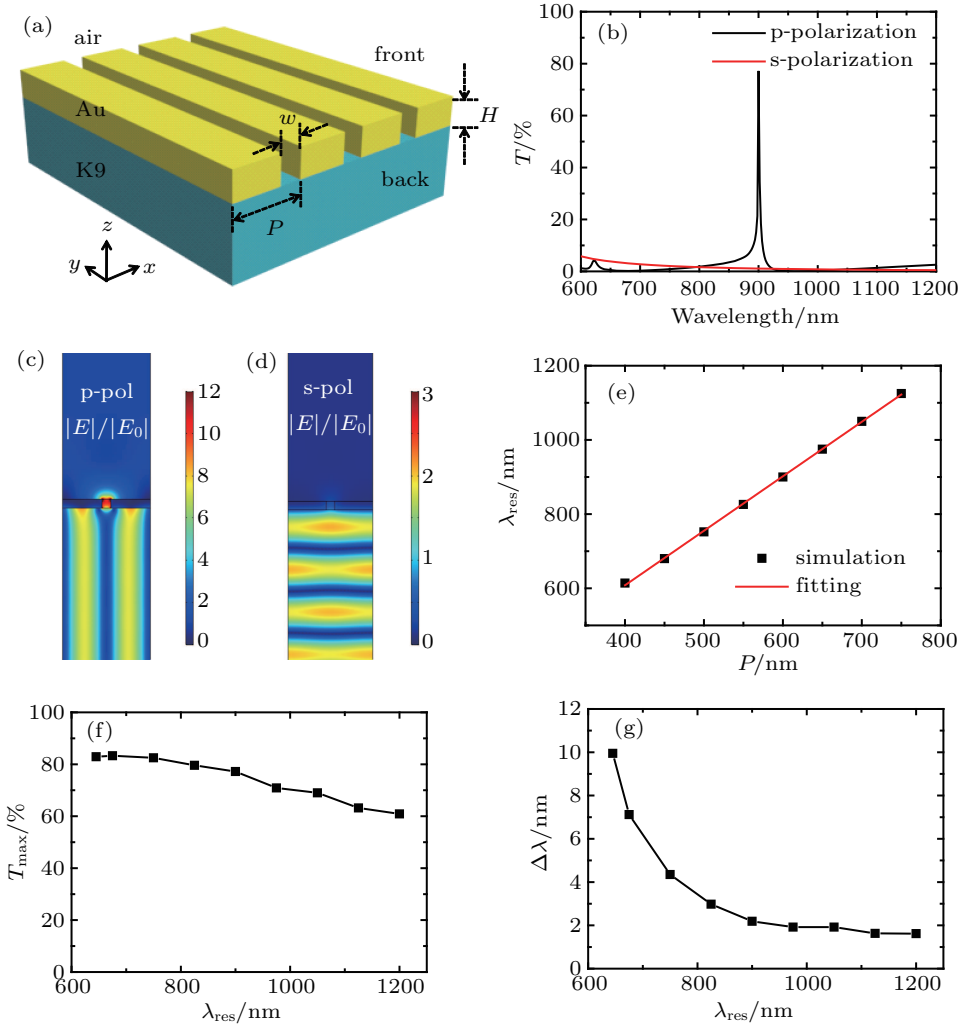


Fig. 1. (a) Schematic of a metallic grating with geometric parameters. (b) Simulation transmission spectra under a p-polarized and an s-polarized incidence. Field distributions ($|E|/|E_0|$) at the first-order resonant wavelength ($\lambda = 900$ nm) under incident light of (c) p-polarizaion and (d) s-polarization. (e) Resonant wavelength as a function of P. (f) Peak transmittance and (g) bandwidth of the metallic filter as functions of the resonant wavelengths.

However, under an s-polarized incident beam, the transmission peaks vanish, and the transmittance is about 1% at $\lambda = 900$ nm, as shown by the red solid line in Fig. 1(b). The reason is that the s-polarized incident beam can not cause field enhancements in the metallic nano-slits. Further simulations show that the field ($|E|^2$) in the single metallic nano-slit under an s-polarized incident light is much weaker (< 24 times) than that under a p-polarized incident light. Due to the weak fields in the metallic nano-slits under an s-polarized incident light, the Wood's anomaly resonance does not happen. In this case, the metallic grating exhibits high reflectance (e.g., $R = 95.4\%$ at $\lambda = 900$ nm), just like a complete gold film ($R = 96.3\%$). The interference of the incident light and the reflected light results in the interference pattern ($|E|/|E_0|$) (parallel to the gold film with period of 300 nm) in the substrate, as shown in Fig. 1(d), which is quite different from that [Fig. 1(c)] caused by the Wood's anomaly.

Additionally, to verify the linear relationship between the resonant wavelength and the period P of the metallic grating in Eq. (1), we plot the first-order resonant wavelength ($m = 1$) as a function of P when $H = 60$ nm and $w = 60$ nm, as shown by the black dots in Fig. 1(e). The red line is a linear fitting curve. It can be seen that the resonant wavelength linearly increases with the period P of the metallic grating. For the red line, the slope is calculated to be 1.5, which is consistent with the refractive index of the glass substrate $n_d = 1.5$. This good consistence strongly verifies the Wood's anomaly resonance. In Fig. 1(f), the peak transmittances of the grating are plotted as a function of resonant wavelengths. The peak transmittances are greater than 60%. At a resonant wavelength of $\lambda = 675$ nm, the transmittance reaches up to 83.3%. The bandwidth of the metallic filter as a function of resonant wavelengths is plotted in Fig. 1(g). It can be observed that the bandwidth of the metallic filter decreases with the wavelengths due to the lower loss of gold in longer wavelengths. The bandwidth is less than 10 nm, and the narrowest bandwidth is as small as $\Delta\lambda_{FWHM} = 1.6$ nm at $\lambda = 1200$ nm.

Unlike conventional metallic filters with localized field

enhancement of SPPs on the metal–dielectric interface,[9–14] the enhanced field generated by the Wood's anomaly in our scheme is mainly distributed in the substrate, which can efficiently reduce the ohmic losses in the metallic film. As a result, the bandwidth is effectively decreased, and the narrowest bandwidth ($\Delta\lambda_{\rm FWHM} \approx 1.6$ nm at $\lambda = 1200$ nm) is smaller than 4% of that in the previous reports ($\Delta\lambda_{\rm FWHM} \geq 40$ nm).[9–17] The bandwidth ($\Delta\lambda_{\rm FWHM} \approx 1.6$ nm at $\lambda = 1200$ nm) is also much narrower than that ($\Delta\lambda_{\rm FWHM} \approx 10$ nm) of commercial dielectric filters (e.g., FB1200-10 in Thorlabs). Moreover, the transmittance ($> 60\%$) is greater than that ($< 50\%$) of commercial dielectric filters (e.g., FB1200-10 in Thorlabs). The corresponding quality factor is as high as $Q = \lambda/\Delta\lambda_{\rm FWHM} = 750$, which is 40 times greater than that in the previous reports.[9–17] By using a silver grating, the bandwidth of our metallic filter can be further narrowed at long wavelengths because of lower ohmic losses in silver.

According to the polarization dependence of the one-dimensional (1D) metallic grating above, it is possible to develop a switchable metallic filter, which has great potential applications in the active digital display and high-density data storage.[23] Herein, an ultrathin two-dimensional (2D) orthogonal metallic grating with different periods is designed as shown in Fig. 2(a). The gold film thickness is also $H = 60$ nm in the simulation. The periods along x-axis and y-axis are $P_1 = 500$ nm and $P_2 = 600$ nm, respectively. On the other hand, the widths along x-axis and y-axis are $w_1 = 80$ nm and $w_2 = 60$ nm, respectively. Figure 2(b) plots simulation transmission spectra under a normal illumination with p-polarization (electric vector parallel to x axis) and s-polarization (electric vector vertical to x axis). It is found that two peak transmittances reach to $\sim 80\%$ with bandwidths of $\Delta\lambda_{\rm FWHM} \approx 3.0$ nm under p-polarized and s-polarized incident beams. Different resonant wavelengths ($\lambda_1 = 750$ nm and $\lambda_2 = 900$ nm) match well with the first-order resonant condition ($m = 1$) of the Wood's anomaly in the metallic grating with different periods of $P_1 = 500$ nm and $P_2 = 600$ nm. As for the 1D gratings, the transmission spectra with the corresponding geometric parameters are simulated in Fig. 2(c) under a p-polarized incident beam. Compared with Fig. 2(c), the 2D orthogonal grating still maintains the same high-transmission and narrowband responses of the 1D metallic gratings. Hence, the filtering property can be switchable by rotating the 2D metallic grating or incident polarization.

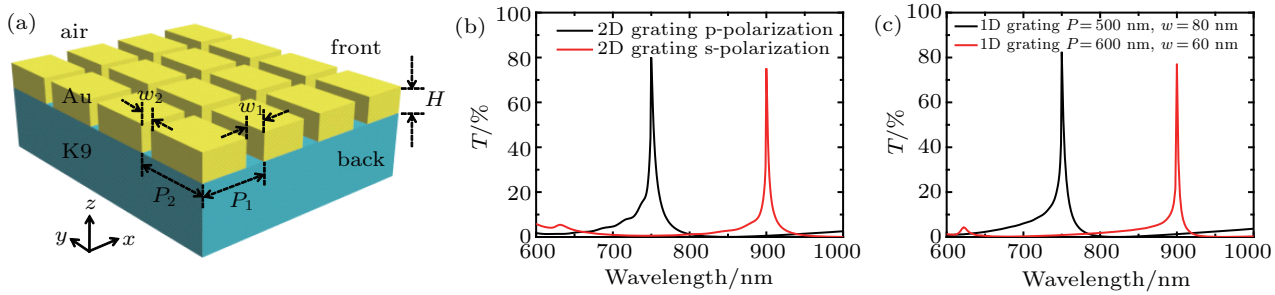


Fig. 2. (a) Schematic of the 2D orthogonal metallic grating with the geometric parameters. (b) Transmission spectra of the 2D orthogonal metallic grating under the p-polarized and s-polarized incidence. (c) Transmission spectra of the 1D metallic grating with the corresponding geometric parameters under the p-polarized incidence.

3. Experiment

In order to verify our theory and simulation, we use focused ion beams (FIB) to fabricated 1D metallic gratings in a gold film with a thickness of 60 nm, which is deposited on a 20 mm×20 mm K9 glass substrate. A scanning electron microscopy (SEM) image and its zoomed-in view are displayed in Figs. 3(a) and 3(b), respectively. The grating comprises 40 nano-slits with a length of 18 μm. The width of the nano-slit is approximatedly $w = 100$ nm. Transmission spectra are measured with a homemade microscope system.[24] A Fianium super-continuum light source illuminates the sample normally from the back side. A Glan–Taylor prism is used to obtain a p-polarized incident light, and a lens (focal length $f = 10$ cm) focuses the polarized light on the sample. A Mitutoyo microscope objective (100× and N. A. = 0.5) collects the transmitted light from the sample, and the collected light is coupled to a spectrograph through a fiber.

A measured transmission spectrum of a gold grating with $P = 400$ nm is shown in Fig. 3(c). The maximum transmittance is $T \approx 48.4\%$ at the transmission peak of $\lambda = 611.5$ nm, and the bandwidth is $\Delta\lambda_{\rm FWHM} \approx 16$ nm. Figure 3(d) depicts a transmission spectrum of a gold grating with $P = 450$ nm. The maximum transmittance is $T \approx 31.7\%$ at the transmission peak of $\lambda = 689.8$ nm, and the bandwidth is $\Delta\lambda_{\rm FWHM} \approx 11$ nm. When the period of the gold grating becomes $P = 500$ nm in the experiment, a transmission peak can be observed at $\lambda = 759.3$ nm in Fig. 3(e). The maximum transmittance is $T \approx 27.8\%$, and the bandwidth is $\Delta\lambda_{\rm FWHM} \approx 10$ nm, which is much smaller than the previous results ($\Delta\lambda_{\rm FWHM} \geq 40$ nm).[9–17]

The experimental transmission spectra exhibit lower transmittances and broader bandwidths than the simulation results. The broader bandwidths originate from the large losses caused by the polycrystalline gold film[25] and the fabrication roughness[26] in the experiments. These large losses also result

in lower transmittances in the experiment. Additionally, the slit width w and thickness H of the nanoslits in the experiment deviate from those (when $H = 60$ nm and $w = 80$ nm) in the simulation. This deviation also leads to lower transmittances in the experiment, which can be observed in the simulation results of Fig. 4. Figure 4 shows that the largest transmittance of the metallic grating with the period $P = 500$ nm is obtained when $H = 60$ nm and $w = 80$ nm.

To decrease the bandwidths of the metallic filter, a monocrystalline metallic (gold or silver) film, which has lower ohmic losses, can be prepared based on an chemically synthesis[27,28] or molecular beam epitaxy (MBE).[29] More importantly, the bandwidth of our metallic filter can be further narrowed by using monocrystalline silver films. By using an FIB technology based on helium[30] or an advanced method based on a lift-off process using high-resolution electron beam lithography (EBL) with a negative-tone hydrogen silsesquioxane (HSQ) resist,[31–33] the slit width can be reliably fabricated to satisfy the designed structural parameters. As a result, the transmittance of the metallic filter could be increased.

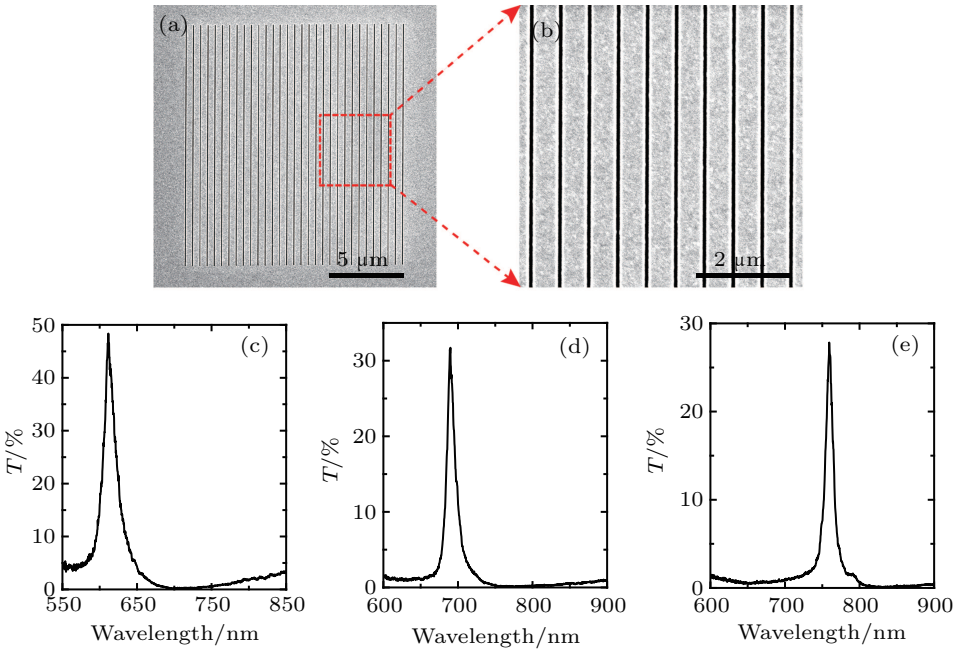


Fig. 3. (a) SEM image of one gold grating with the period of $P = 400$ nm. (b) Zoomed-in view of the sample. Experimental transmission spectra of the samples with (c) $P = 400$ nm, (d) $P = 450$ nm, and (e) $P = 500$ nm.

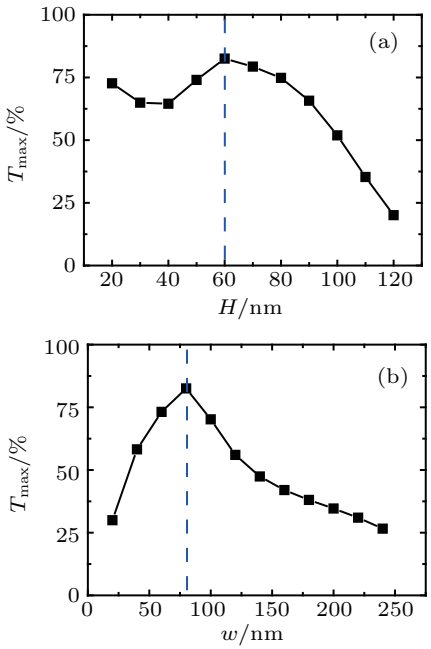


Fig. 4. Transmittance of the gold grating as functions of (a) the thickness H when $P = 500$ nm, $w = 80$ nm and (b) the slit width w when $P = 500$ nm, $H = 60$ nm.

A 2D orthogonal grating is also fabricated in a 60 nm-thick gold film on a 20 mm ×20 mm K9 glass substrate. A SEM image of the 2D orthogonal gold grating with $P_1 = 400$ nm and $P_2 = 430$ nm and its zoomed-in view are displayed in Figs. 5(a) and 5(b), respectively. The numbers of nano-slits in each dimension are both 40, and the size of the 2D grating is 18 μm ×18 μm. The width of the nano-slits is approximately $w = 100$ nm. An experimental transmission spectrum of the sample is depicted in Fig. 5(c) under a p-polarized incident light. A transmission peak appears at $\lambda = 618.7$ nm with a maximum transmittance of $T \approx 39\%$ and a bandwidth of $\Delta\lambda_{\mathrm{FWHM}} \approx 38$ nm. Figure 5(d) depicts an experimental transmission spectrum of the sample under an s-polarized incident light. A resonant wavelength is observed at 659.9 nm with a maximum transmittance of $T \approx 39\%$ and a bandwidth of $\Delta\lambda_{\mathrm{FWHM}} \approx 30$ nm. When the angle between x-axis and the polarization of the incident beam becomes 45°, it can be observed that there are two transmission peaks at 618.7 nm and 658.3 nm in Fig. 5(e). The maximum transmittance and the bandwidth of the peak at the shorter wave-

length ($\lambda = 618.7$ nm) are $T \approx 26\%$ and $\Delta\lambda_{\rm FWHM} \approx 42$ nm, respectively. At the same time, the maximum transmittance and the bandwidth at the longer wavelength ($\lambda = 658.3$ nm) are $T \approx 25\%$ and $\Delta\lambda_{\rm FWHM} \approx 32$ nm, respectively. The differences between experimental results and simulation data stem from the fabrication imperfections and limit as discussed above. As a result, the transmission spectra can be adjusted by rotating the incident polarization effectively.

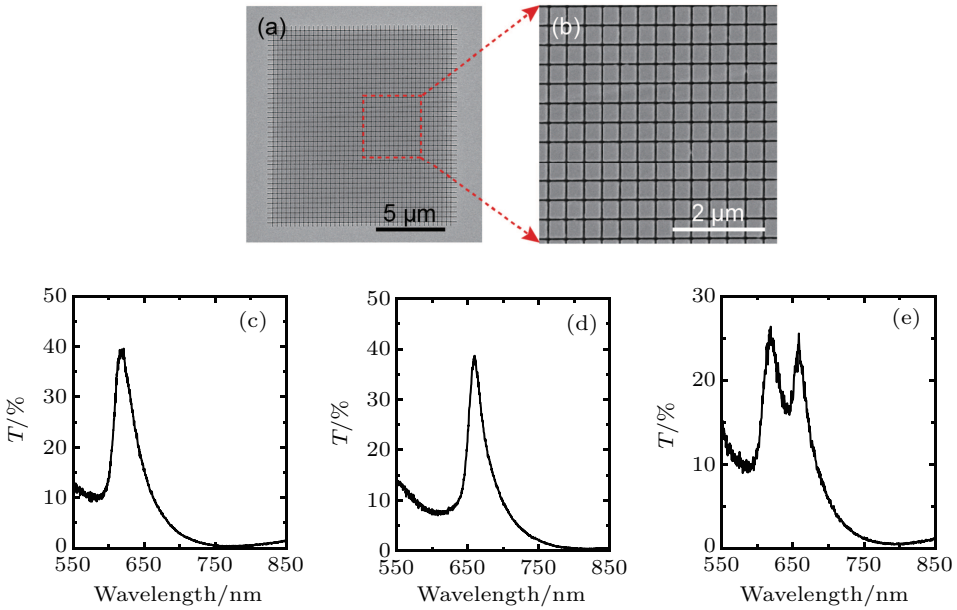


Fig. 5. (a) SEM image of the 2D orthogonal grating with the periods of $P_1 = 400$ nm and $P_2 = 430$ nm. (b) Zoomed-in SEM image of the 2D orthogonal grating. Experimental transmission spectra of the samples under (c) p-polarization, (d) s-polarization, and (e) 45° polarization incident beam illumination.

4. Conclusion

In summary, by employing both strong field enhancements in metallic nano-slits and the Wood's anomaly in an ultrathin ($H = 60$ nm) single-layer gold grating, a metallic filter with an extra-narrow bandwidth was demonstrated. Our filter was 40% thinner than the previous dielectric and metallic filters (thickness ≥ 150 nm).[9–17] Unlike localized field enhancement of SPPs on metal–dielectric interfaces, the Wood's anomaly in the ultrathin single-layer gold grating led to large field enhancements in the substrate, which efficiently reduced ohmic losses in the metals. The narrowest transmission bandwidth (transmittance $> 60\%$) at $\lambda = 1200$ nm was as small as $\Delta\lambda_{\rm FWHM} \approx 1.6$ nm, which was smaller than 4% of that ($\Delta\lambda_{\rm FWHM} \geq 40$ nm) in the previous reports.[9–17] The corresponding quality factor was as high as $\lambda/\Delta\lambda_{\rm FWHM} = 750$, which was 40 times greater than that in the previous reports.[9–17] The performances (bandwidth, transmittance, and thickness) of the metallic filter were even better than commercial dielectric filters (e.g., FB1200-10 in Thorlabs). Based on the polarization-dependent property of the metallic grating, the transmission spectra could be adjusted by rotating the incident polarization or the the metallic grating. In the experiment, metallic gratings were fabricated on a single-layer gold film. A narrowband metallic filter with a bandwidth of $\Delta\lambda_{\rm FWHM} = 10$ nm, which was smaller than 25% of that ($\Delta\lambda_{\rm FWHM} \geq 40$ nm) in the previous reports,[9–17] was demonstrated. This extra-narrowband metallic filter with polarization-dependent properties would offer great potential for the practical applications in optical display technology, optical information processing, hyperspectral imaging, and high-density optical storage.

References

[1] Zheng B Y, Wang Y M, Nordlander P and Halas N J 2014 *Adv. Mater.* **26** 6318
[2] Nguyenhuu N, Cada M, Pištora J and Yasumoto K 2014 *J. Lightwave Technol.* **32** 4079
[3] Zhu X L, Vannahme C, Højlundnielsen E, Mortensen N A and Kristensen A 2016 *Nat. Nanotechnol.* **11** 325
[4] Wang W B, Zhang F J, Du M D, Li L L, Zhang M, Wang K, Wang Y S, Hu B, Fang Y and Huang J S 2017 *Nano Lett.* **17** 1995
[5] Nagasaki Y, Suzuki M and Takahara J 2017 *Nano Lett.* **17** 7500
[6] Proust J, Bedu F, Gallas B, Ozerov I and Bonod N 2016 *ACS Nano* **10** 7761
[7] Kristensen A, Yang J K, Bozhevolnyi S I, Link S, Nordlander P, Halas N J and Mortensen N A 2017 *Nat. Rev. Mater.* **2** 16088
[8] Chen J J, Gan F Y, Wang Y J and Li G Z 2018 *Adv. Opt. Mater.* **6** 61701152
[9] Burgos S P, Yokogawa S and Atwater H A 2013 *ACS Nano* **7** 10038
[10] Do Y S, Park J H, Hwang B Y, Lee S M, Ju B K and Choi K C 2013 *Adv. Opt. Mater.* **1** 133
[11] Yokogawa S, Burgos S P and Atwater H A 2012 *Nano Lett.* **12** 4349
[12] Miyata M, Hatada H and Takahara J 2016 *Nano Lett.* **16** 3166
[13] Cheng F, Gao J, Luk T S and Yang X D 2015 *Sci. Rep.* **5** 11045
[14] Shah Y D, Grant J, Hao D, Kenney M, Pusino V and Cumming D R 2018 *Acs Photon.* **5** 663
[15] Xu T, Wu Y K, Luo X G and Guo L J 2010 *Nat. Commun.* **1** 59
[16] Diest K, Dionne J A, Spain M and Atwater H A 2009 *Nano Lett.* **9** 2579
[17] Li Z Y, Butun S and Aydin K 2015 *ACS Photon.* **2** 183

[18] Liu H T and Lalanne P 2008 *Nature* **452** 728
[19] Kim K Y, Chong X Y, Ren F H and Wang A X 2015 *Opt. Lett.* **40** 5339
[20] Gao H, Mcmahon J M, Lee M H, Henzie J, Gray S K, Schatz G C and Odom T W 2009 *Opt. Express* **17** 2334
[21] Zhang Y F, Wang H M, Liao H M, Li Z, Sun C W, Chen J J and Gong Q H 2014 *Appl. Phys. Lett.* **105** 231101
[22] Johnson P B and Christy R W 1972 *Phys. Rev. B* **6** 4370
[23] Heydari E, Sperling J R, Neale S L and Clark A W 2017 *Adv. Funct. Mater.* **27** 1701866
[24] Chen J J, Sun C W, Rong K X, Li H Y and Gong Q H 2015 *Laser Photon. Rev.* **9** 419
[25] Bao Y M, Liang H, Liao H M, Li Z, Sun C W, Chen J J and Gong Q H 2017 *Plasmonics* **12** 1425
[26] Sun C W, Rong K X, Wang Y J, Li H Y, Gong Q H and Chen J J 2016 *Nanotechnology* **27** 065501
[27] Huang J S, Callegari V, Geisler P, Brüning C, Kern, J, Prangsma J C, Wu X F, Feichtner T, Ziegler J, Weinmann P, Kamp M, Forchel A, Biagioni P Sennhauser U and Hecht B 2010 *Nat. Commun.* **1** 150
[28] Wang C Y, Chen H Y, Sun L Y, Chen W L, Chang Y M, Ahn H, Li X Q and Gwo S 2015 *Nat. Commun.* **6** 7734
[29] Bhatta U M, Dash J K, Rath A and Satyam P V 2009 *Appl. Surf. Sci.* **256** 567
[30] Chen K, Razinskas G, Vieker H, Gross H, Wu X F, Beyer A, Gölzhäuser A and Hecht B 2018 *Nanoscale* **10** 17148
[31] Zheng M J, Chen Y Q, Liu Z, Liu Y, Wang Y S, Liu P, Liu Q, Bi K X, Shu Z W, Zhang Y H and Duan H G 2019 *Microsyst. Nanoeng.* **5** 54
[32] Chen Y Q, Xiang Q, Li Z Q, Wang Y S, Meng Y H and Duan H G 2016 *Nano Lett.* **16** 3253
[33] Duan H G, Hu H L, Kumar K, Shen Z X and Yang K W 2011 *ACS Nano* **5** 7593